Müller matrix measurements

Adrian Casado Eide Svein Åmdal

24. February 2020

Abstract: In this report we plot numerically the Müller matrix elements of various optical systems. Using a differential decomposition method the logarithm of the Müller matrices together with its fluctuations are plotted and results discussed. The optical elements behave close to the theory in the energy range of approximately 1.5eV−3eV.

1 Introduction

This is a report of the results of a laboratory session in the course TFY4200: "Optics - Advanced course" at NTNU, spring 2020. Making use of a commercial ellipsometer, we measured Müller matrix elements as a function of frequency for a selection of (known) optical elements.

2 Theory

[1] For electromagnetic waves, electric ($\boldsymbol{D}$) and magnetic ($\boldsymbol{B}$) fields are directed perpendicular to each other and perpendicular to the direction of propagation. If there is a macroscopic tendency for the fields to be oriented a certain way in the plane, the light has some degree of polarization. In this lab, we mainly consider fully polarized light. The direction of the $\boldsymbol{D}$-field is the direction of polarization. Note that this direction need not be constant in space (linear polarization); there may in fact be a phase difference between the x- and y-components of $\boldsymbol{D}$ yielding elliptical polarization.

A Stokes vector (really, a 4x1 column matrix) has four components pertaining to polarization in different directions, being

$$\boldsymbol{S} = \begin{bmatrix} I \\ Q \\ U \\ V \end{bmatrix} = \begin{bmatrix} I_x + I_y \\ I_x - I_y \\ I_{+45^\circ} - I_{-45^\circ} \\ I_{\text{right circ.}} - I_{\text{left circ.}} \end{bmatrix}, \tag{1}$$

Where I_q is the intensity measured in q-direction. The Stokes parameters represent:

- I: Total intensity
- Q: Linear polarization along the x and y axes. $Q = 1 \implies$ polarization in $\hat{x}$. $Q = -1 \implies$ polarization in $\hat{y}$.
- U: Linear polarization along the $\pm 45^\circ$ directions, with $U = \pm 1$ being the extreme cases.
- V: $V = \pm 1 \implies$ Complete left-handed or right-handed circular polarization.

Optical elements can alter the polarization state. A Müller matrix (4x4) is a representation of how an optical element alters the polarization state that is represented by a Stokes vector. Thus, the polarization state exiting an optical element represented by the Müller matrix $\boldsymbol{M}$ can be described by

$$\boldsymbol{S}_{\text{out}} = \boldsymbol{M}\boldsymbol{S}_{\text{in}}, \tag{2}$$

and a polarization state exiting from a sequence of N optical elements can similarly be described by

$$\boldsymbol{S}_{\text{out}} = \prod_{n=1}^{N} \boldsymbol{M}_n \boldsymbol{S}_{\text{in}}. \tag{3}$$

With knowledge of $\boldsymbol{S}_{\text{in}}$ and measurement of $\boldsymbol{S}_{\text{out}}$, one can determine the elements of the Müller matrix of some unknown system.

For an ideal linear polarizer the Müller matrix becomes

$$\boldsymbol{M}_{\text{Lin. pol.}} = \begin{bmatrix} 1 & 1 & 0 & 0 \\ 1 & 1 & 0 & 0 \\ 0 & 0 & 0 & 0 \\ 0 & 0 & 0 & 0 \end{bmatrix}. \tag{4}$$

The Müller matrix for a 45° quarter wave plate linear retarder becomes[1, p. 160]

$$\boldsymbol{M}_{\mathbf{45^\circ}} = \begin{bmatrix} 1 & 0 & 0 & 0 \\ 0 & 0 & 0 & -1 \\ 0 & 0 & 1 & 0 \\ 0 & 1 & 0 & 0 \end{bmatrix}. \tag{5}$$

In addition there is the Müller matrix for the general retarder

$$\boldsymbol{M}_R = \begin{bmatrix} 1 & 0 & 0 & 0 \\ 0 & 1 & 0 & 0 \\ 0 & 0 & \cos\delta & \sin\delta \\ 0 & 0 & -\sin\delta & \cos\delta \end{bmatrix}, \tag{6}$$

where δ is the phase difference. Finally for the diattenuator

$$\boldsymbol{M}_D = \frac{1}{2}\begin{bmatrix} T_x + T_y & T_x - T_y & 0 & 0 \\ T_x - T_y & T_x + T_y & 0 & 0 \\ 0 & 0 & 2\sqrt{T_x T_y} & 0 \\ 0 & 0 & 0 & 2\sqrt{T_x T_y} \end{bmatrix} \tag{7}$$

Where $T_x = |t_x|^2$ and $T_y = |t_y|^2$ are the Fresnel transmission probabilities in the x and y direction respectively.

As suggested by eq. (3), a Müller matrix may be decomposed into individual components. Another possible decomposition technique is *differential* decomposition.

Let $\boldsymbol{M}(z)$ describe the Müller matrix in a medium between $z = d$ and $z = 0$, where d is the thickness of the sample, then by eq. (2),

$$\boldsymbol{S}(z) = \boldsymbol{M}(z)\boldsymbol{S}(0). \tag{8}$$

Using equation 6.174 in [1] and differentiating eq. (8) with respect to z, we obtain

$$\boldsymbol{m}\boldsymbol{S}(z) = \frac{\mathrm{d}\boldsymbol{M}(z)}{\mathrm{d}z}\boldsymbol{S}(0), \tag{9}$$

where $\boldsymbol{m}$ is the differential Müller matrix. Inserting eq. (8) into eq. (9) and eliminating $\boldsymbol{S}(0)$ we arrive at a differential equation for $\boldsymbol{M}(z)$:

$$\frac{\mathrm{d}\boldsymbol{M}}{\mathrm{d}z} = \boldsymbol{m}\boldsymbol{M}. \tag{10}$$

Assuming a homogeneous sample, eq. (10) can be solved exactly yielding the final result

$$\boldsymbol{L} := \boldsymbol{m}d = \ln \boldsymbol{M}_{\boldsymbol{S}}, \tag{11}$$

where $\boldsymbol{M}_{\boldsymbol{S}}$ is the Müller matrix of the sample.

The differential decomposition matrix $\boldsymbol{L}$ is useful for identifying birefringence and dichroism. Following the method of [1], one arrives at a functional understanding of what $\boldsymbol{L}$ entails in practice. Namely,

$$\boldsymbol{M}_D = \begin{bmatrix} 0 & d_{xy} & d_{\pm 45} & d_{lr} \\ d_{xy} & 0 & \delta_{lr} & -\delta_{\pm 45} \\ d_{\pm 45} & -\delta_{lr} & 0 & \delta_{xy} \\ d_{lr} & \delta_{\pm 45} & -\delta_{xy} & 0 \end{bmatrix}, \tag{12}$$

where d_{xy} is the diattenuation for x- and y (linear) polarizations, $d_{\pm 45}$ is the diattenuation for $+45°$ and $-45°$ (linear) polarizations, d_{lr} is the diattenuation for left- and right-circular polarizations, and $\delta_{\dots}$ is the phase delay in its respective polarization directions.

Differential decomposition is performed numerically with an algorithm based on [2] and [3].

3 Experimental layout

Various samples was placed in between the light source and the detector of an ellipsometer. The light source is a $150W$ Xe-lamp. The radiation emanating from the resulting hot plasma is frequency filtered and focused using an internal imaging system, and emitted as light rays. (This process takes place in a 'black box'.) For each internal reflection there is phase shift for both $\boldsymbol{s}$ and $\boldsymbol{p}$ directions, which can be fine tuned.

The ellipsometer was calibrated with an "empty", calibrating measurement. Then, samples were measured, and their Müller matrices and differential decompositions extracted numerically. The ellipsometer measures a diffracted beam, yielding a frequency spectrum of all matrix elements.

The first sample was a dichroic polymer based linear polarizer. Intensity measurements for various orientations were performed.

The second sample was an achromatic quarter wave plate. We aligned the fast axis with the linear polarizer, retrieving a retarder (cf. section 4). Thereafter, we measured a 45° rotated sample, where we predict to measure circular polarization.

The third sample was a Glan-Thompson polarizer, i.e. a prism polarizer. A Glan-Thompson is an approximate ideal linear polarizer. We also combined Glan-Thompson with the quarter waveplate. Fourthly, we investigated a Rochon polarizer. It consists of a MgF_2-crystal, which we expect to function for all applied wavelengths due to the crystal being transparent for a large range of wavelengths.[4]

Finally, we used an LCVR (Liquid Crystal Variable Retarder) without voltage as a substrate. Thereafter, we fine tuned the voltage to 6 and $12V$ in order to observe the variable retardance.

Only some of the measurement data are included in this report for brevity.

4 Results

The calculated Müller matrices for some measurements are given in figs. 1 to 4. In these plots, the sub-figure in position (i,j) is the dimensionless Müller matrix component M_{ij} as a function of incoming photon energy (eV).[1] Note that the (1,1)-sub-figure of each Müller matrix is replaced by the

[1] These were plotted with pre-fabricated code, and adding individual axis lables was nontrivial.

total intensity measured with respect to the ambient calibration measurement. The Müller matrix components are all normalized with respect to unit intensity (as they should), but now figs. 1 to 4 also contains information about the absorbance of the samples.

Using the differential decomposition scheme, we recovered decomposition matrices given by figs. 5 to 8. The blue lines indicate the decomposition $\boldsymbol{L}$ while the red lines indicate the standard deviation. The horizontal axes once again represents incoming photon energies in eV.[2]

We note that fig. 1 does indeed resemble the matrix given by eq. (6) in a sufficiently low energy range, with a phase difference δ that depends on the applied frequency. We also note that in the range of reasonable model fit, fig. 5 tells the story of a phase difference between the x- and y-directions, like one expects from a xy-aligned wave plate.

Figure 2 rather resembles eq. (5) with a rotation of $-45°$, while fig. 6 emphasizes the phase difference between $+45$ and $-45°$ polarizations.

Figure 3 resembles eq. (4) with a notably large absorbance. Figure 7 indicates substantial values of d_{xy}, indicating substantial diattenuation in the axes aligned with the incoming polarization.

Finally, fig. 4 is obtained by multiplying the Müller matrix of figure 2 and 3 together, achieving $M_{12} = 1$, $M_{41} = M_{42} = -1$ and 0 otherwise, as numerically indicated by fig. 4. Indicating that fig. 4 is a composite system of a Glan-Thompson and a quarter wave plate, which is consistent.

5 Discussion

The previous comparison between results and idealized Müller matrices are functionally valid, but they differ in the details. For instance, the comparisons are most valid in certain frequency ranges, generally on the lower end of the plotted spectrum. In figs. 1 to 3, the comparison is most valid for $E \lesssim 3\text{eV}$. Not surprisingly, this corresponds to the region where transmittance is large (meaning the normalized intensity is relatively close to 1. In fig. 3 there is also some prevalent noise on low frequencies. This noise is, however, much smaller than the large-frequency dependent irregularities in figs. 1 and 2.

The transmittance of fig. 4 is jarring, and leaves a lot of room for noise and uncertainty.

In figs. 5 and 6, we recognize low decomposition uncertainty everywhere apart from low frequencies. Along with the valid frequency range above, we may identify the achromatic quarter-wave plate to behave quite ideally in the range of energies $1.5\text{eV}-3\text{eV}$.

Observing the fluctuations in fig. 3, the Glan-Thompson polarizer also seems to behave most ideally in this same energy range.

In figs. 7 and 8, we observe that the fluctuations L_u marked in red are mostly of the same order or larger than the mean values L_m marked in blue. We would expect the fluctuations to be smaller than the mean values themselves, in order to indicate perturbative convergence. This is not the case here, most likely due to measurement noise. It may also be the case that the perturbative expansion simply does not converge, or that the normalization measurement is inconsistent with the later measurements.

Some of the Müller matrix elements leave the decomposition algorithm to calculate the logarithm of a negative number. In these cases, the real part of the principal complex logarithm is chosen, but this is certainly a source of error.

It is known that for a Müller matrix $\boldsymbol{M}$ its matrix elements should be in-between -1 and 1, this is not the case for any of our figures. It is likely due to faulty normalization, or that the normalization is only valid in a certain frequency range.

According to eq. (11) the logarithm of the Müller matrix $\boldsymbol{L}$ which we measured is related to the thickness of the sample d. We suspect that the large values for some of these Müller matrix elements is due to this thickness. Either d is too large to neglect the propagation through the optical element, the sample is non-homogeneous in the propagation direction, or d is variable across the sample.

We also expect that there may have been some effects of absorption in the sample, causing the sum of the reflection and transmission coefficients being different from unity - which in turn will make the empirical results differ from the theoretical ones. However we assume that the effects of absorption

[2] Again, adding individual axis labels was nontrivial.

is small compared with other sources of error discussed. Since the instrument used for measurements was calibrated prior to the sampled measurements we expect the general measurement uncertainties from the ellipsometer to be negligible.

6 Exercises

1.

A Babinet-Soleil compensator is a zero order retarder. That is an optical, polarizing and birefringent device that satisfies causality. It consists of two birefringent plates of perpendicular optic axes, also perpendicular to the incoming beam. The thickness of one of the plates may be altered mechanically, giving a tunable phase shift.

The Wollaston prism is an optical device that manipulates polarized light in the sense that is splits the incoming beam into two outgoing, linearly polarized beams with orthogonal polarization. Two triangular, birefringent prisms with orthogonal optic axes are cemented together. Thus the phase shift may be determined by the location of the incoming beam.

2.

A Glan-Thompson polarizer is an optical device that consists of two prisms each being a birefringent crystal with parallel optical axis, there will be discontinuities in the optical paths in the interface between the two regions, depending on the refractive indices of the two prisms respectively. If the internal angle of incidence θ_0 is in some specific region

$$\frac{n_g}{n_o} < \sin\theta_0 < \frac{n_g}{n_e}. \tag{13}$$

Where n_g is the refractive index of the cement gap in between the two prisms and n_e, n_o are the refractive indices in the extraordinary and ordinary directions respectively.
Then the GT-polarizer is such that the ordinary component will be totally reflected, $r_{po} = 1$. The polarizer also has a high extinction ratio, meaning that a lot of energy is lost during the propagation.

3.

One typical IR-polarizer is a *wire-grid* polarizer. The polarization is due to an anisotropic ϵ from asymetric microstructure. The polarization component parallel to the wires, are absorbed (in the process of exciting electron oscillations along the wires). This remains true even for IR-frequencies.

Polymer sheet polarizers can be used for near-IR. Polymer sheet polarizers function much like wire-grids. The polymers are long molecules that are stretched out during manufacturing, and this asymmetric microstructure results in anisotropic ϵ.

Polarizers based on elongated silver nanoparticles[5] is also used in the near-IR regime, and has applications in fiber-optics. The principle is the same.

4.

A *photo-elastic modulator* makes use of the effect of *photoelasticity* to specify outgoing polarization state. I.e. a dielectric function ϵ that depends on mechanical displacement. Photoelasticity is a tensorial quantity, so it (P_{ijkl}) captures changes in ϵ_{ij} due to a displacement in $\hat{k}$ upon a differential displacement in $\hat{l}$. In short, one controls the optic axis with mechanical deformation of a photoelastic material.

A *ferro-electric liquid crystal* is a liquid material that shows ferromagnetic domain structure. Each domain is optically uniaxial, and the domain walls may be manipulated by an external electric field. [6] This allows precise alteration of the relatve optical path length through differently oriented uniaxial materials, meaning control over the relative phase shift.

A *nematic variable liquid crystal retarder* contains elecrically dipolar molecules, and upon applying an external electric field, the molecules aligns (presumably following the theory of para-electricity, thus having a regime of linear relation to the applied field). These molecules also cause anisotropy in ϵ for similar reasons as above.[7]

An *electro-optic active retarder* has birefringence produced by an applied electric field (either linear Pockels, or quadratic Kerr effects), and is *active* in the sense that the wave passing through may be amplified.

5.

5.1.

The Lu-Chipman non-polarizing decomposition makes it possible to decompose a Mueller matrix $\boldsymbol{M}$ into a product of a retarder and a diattenuator.

$$\boldsymbol{M} = \boldsymbol{M}_R \boldsymbol{M}_D \tag{14}$$

The structure of which we will not come deeper into in this article. The advantage of such a decomposition is that it is easily applicable given that the diattenuator matrix $\boldsymbol{M}_D$ is invertible.

5.2.

Ossikovski retarder decomposition is of the form

$$\boldsymbol{M} = \boldsymbol{M}_{R1} \boldsymbol{M}_{\Psi\Delta} \boldsymbol{M}_{R2}^T \tag{15}$$

Where $\boldsymbol{M}_{R1}$ and $\boldsymbol{M}_{R2}$ are two linear retarders and $\boldsymbol{M}_{\Psi\Delta}$ are an 'ellipsometric-type' Mueller matrix. The advantage of such a decomposition is that it gives a simple physical interpretation: Two waveplates and a reflecting surface. Another advantage is that this decomposition also works for singular Mueller matrices $\boldsymbol{M}$.

5.3.

There is also another more general form of the Lu-Chipman decomposition, namely that of a depolarizing Mueller matrix $\boldsymbol{M}$.

$$\boldsymbol{M} = \boldsymbol{M}_\Delta \boldsymbol{M}_R \boldsymbol{M}_D \tag{16}$$

Where $\boldsymbol{M}_\Delta$ is the depolarizing matrix and $\boldsymbol{M}_R$ and $\boldsymbol{M}_D$ are the retarder and diattenuator matrices as before. The advantage of such a decomposition is that it is a lot more general than the first case and therefore applicable to much more cases.

6.

A spatial light modulator is an optical device that impose changes in the spatial modulation of a refractive beam. An SLM is used extensively in holographic data storage to encode information. It is also used in the measurement and shaping of ultrafast laser pulses. Since the SLM itself can be used to modulate waves, thereby changing its form and detecting it. This is useful because it thereby becomes possible to transform the wavelet into a transform limited pulse, where we have optimized the peak power.

7.

A wave-plate is a rectangular prism with frequency-dependent refractive indices. A Fresnel-prism is the same material cut to have the off-axis positions such that the optical path length of a diffracted beam (higher frequency) coincides with the central beam. Effectively, this means that each small range of wavelengths has a tailored path length, and therefore the phase difference is nearly wavelength-independent.

Deviations may be due to cuts being finite in size, and each optical path length therefore pertaining to a finite range of frequencies. It may also be limited by the spatial coherence of the source.

8.

We may as well assume that the polarizer is linear and aligned in the x-direction, and that the Poincaré sphere is parametrized in standard coordinates where θ corresponds to the angle of rotation of the polarization ellipse from the x-axis. We may then take the rotating achromatic retarder to produce an angle $\theta = \omega t$ with the x-axis. By sending in unpolarized[3] light represented by a Stokes vector, and sending it through the specified optical system, we identify through numerical calculation (see appendix A)

$$\boldsymbol{R}(-\theta)\boldsymbol{M}_{\text{ret}}\boldsymbol{R}(\theta)\boldsymbol{M}_{\text{pol}}\begin{bmatrix}1\\0\\0\\0\end{bmatrix} = \underbrace{\begin{bmatrix}0.5\\0.3337\cos 4\theta + 0.1663\\0.3337\sin 4\theta\\-0.4711\sin 2\theta\end{bmatrix}}_{\text{For } \delta = 132^\circ} = \underbrace{\begin{bmatrix}0.5\\0.3249\cos 4\theta + 0.1751\\0.3249\sin 4\theta\\-0.477\sin 2\theta\end{bmatrix}}_{\text{For } \delta = 90^\circ}. \tag{17}$$

From eq. (5.88b) in [1] we have

$$\epsilon = \frac{1}{2}\arcsin\left(\frac{V}{I}\right), \tag{18}$$

where ϵ does *not* refer to any dielectric function, but to the parametrization angle of the Poincaré sphere. Regardless of which of the angles δ is chosen, we get that

$$\epsilon = 1/2\arcsin\left(-0.9422\sin(2\theta)\right) \approx -\theta. \tag{19}$$

In total we have the time variations $\theta = \omega t$ and $\epsilon \approx -\omega t$. This traces out a closed curve on the Poincaré sphere. The curve starts out at linear x-polarization, makes a curved line[4] to left-circular polarization, a similar curve to linear y-polarization, then to right-circular polarization and then returning to its starting point. Without drawing any pictures, the closest description I can give is a "tennis ball-like" shape drawn out on the circle.

7 Conclusion

We measured various optical samples and plotted the different Müller matrices including their logarithms and its fluctuations using the differential decomposition method for these samples. The numerical Müller matrices are consistent with the theoretical Müller matrices as explained in section section 4 in the energy range of 1.5eV−3eV. We retrieved an unexpectedly large fluctuation in $\boldsymbol{L}$ being of the same order as $\boldsymbol{L}$ itself. We conclude that this is most likely due to measurement noise, or some other factor that makes the differential decomposition algorithm diverge.

[3] Or any other polarization state. It does not matter, for we assume the polarizer is ideal.

[4] Curved, as in *not* the shortest path in the spherical geometry

References

[1] H. Arwin, "Thin film optics and polarized light," 2016.

[2] R. Ossikovski, "Differential matrix formalism for depolarizing anisotropic media," *Opt. Lett.*, vol. 36, no. 12, pp. 2330–2332, Jun 2011. [Online]. Available: http://ol.osa.org/abstract.cfm?URI=ol-36-12-2330

[3] S. Kumar, H. Purwar, R. Ossikovski, I. A. Vitkin, and N. Ghosh, "Comparative study of differential matrix and extended polar decomposition formalisms for polarimetric characterization of complex tissue-like turbid media," *Journal of Biomedical Optics*, vol. 17, no. 10, pp. 1 – 12, 2012. [Online]. Available: https://doi.org/10.1117/1.JBO.17.10.105006

[4] "Magnesium fluoride." [Online]. Available: https://en.wikipedia.org/wiki/Magnesium_fluoride

[5] Corning Inc., December 2006, https://web.archive.org/web/20071012211246/http://www.corning.com/docs/specialtymaterials/pisheets/Pi201.pdf (archived).

[6] N. A. Clark and S. T. Lagerwall, "Submicrosecond bistable electro-optic switching in liquid crystals," *Applied Physics Letters*, vol. 36, no. 11, pp. 899–901, 1980. [Online]. Available: https://doi.org/10.1063/1.91359

[7] ThorLabs, "Full-wave liquid crystal variable retarders / wave plates." [Online]. Available: https://www.thorlabs.com/newgrouppage9.cfm?objectgroup_id=6339

A
MATLAB code

```
%lab1_8.m
%Svein Aamdal

syms theta delta;

%Assume the incoming beam is unpolarized
S_in = [1 0 0 0];

%Assume the polarizer is linear in x
M_pol = 1/2 .* [1, 1, 0, 0; 1, 1, 0, 0; 0, 0, 0, 0; 0, 0, 0, 0];
%Assume the retarder to be simple, ideal and linear
M_ret = [1, 0, 0, 0; 0, 1, 0, 0; 0, 0, cos(delta), sin(delta); 0, 0, -sin(delta),
    cos(delta)];
%Rotation matrix, to rotate the retarder by an angle theta = omega*t
R = [1, 0, 0, 0; 0, cos(2*theta), sin(2*theta), 0; 0, -sin(2*theta), cos(2*theta), 0; 0, 0,
    0, 1];
R_inv = [1, 0, 0, 0; 0, cos(-2*theta), sin(-2*theta), 0; 0, -sin(-2*theta), cos(-2*theta),
    0; 0, 0, 0, 1];

M_rot = R_inv * M_ret * R;
S_out = M_rot * M_pol * transpose(S_in);

S_1 = subs(S_out, delta, 132*180/pi); %132 deg phase shift
S_2 = subs(S_out, delta, 90*180/pi); %90 deg phase shift

%Get rid of cos of (very) large fraction, approximate to 4 decimals
%Also algebraic simplification
S_1 = vpa(simplify(vpa(S_1, 4)), 4);
S_2 = vpa(simplify(vpa(S_2, 4)), 4);

disp(S_1);
disp(S_2);
```

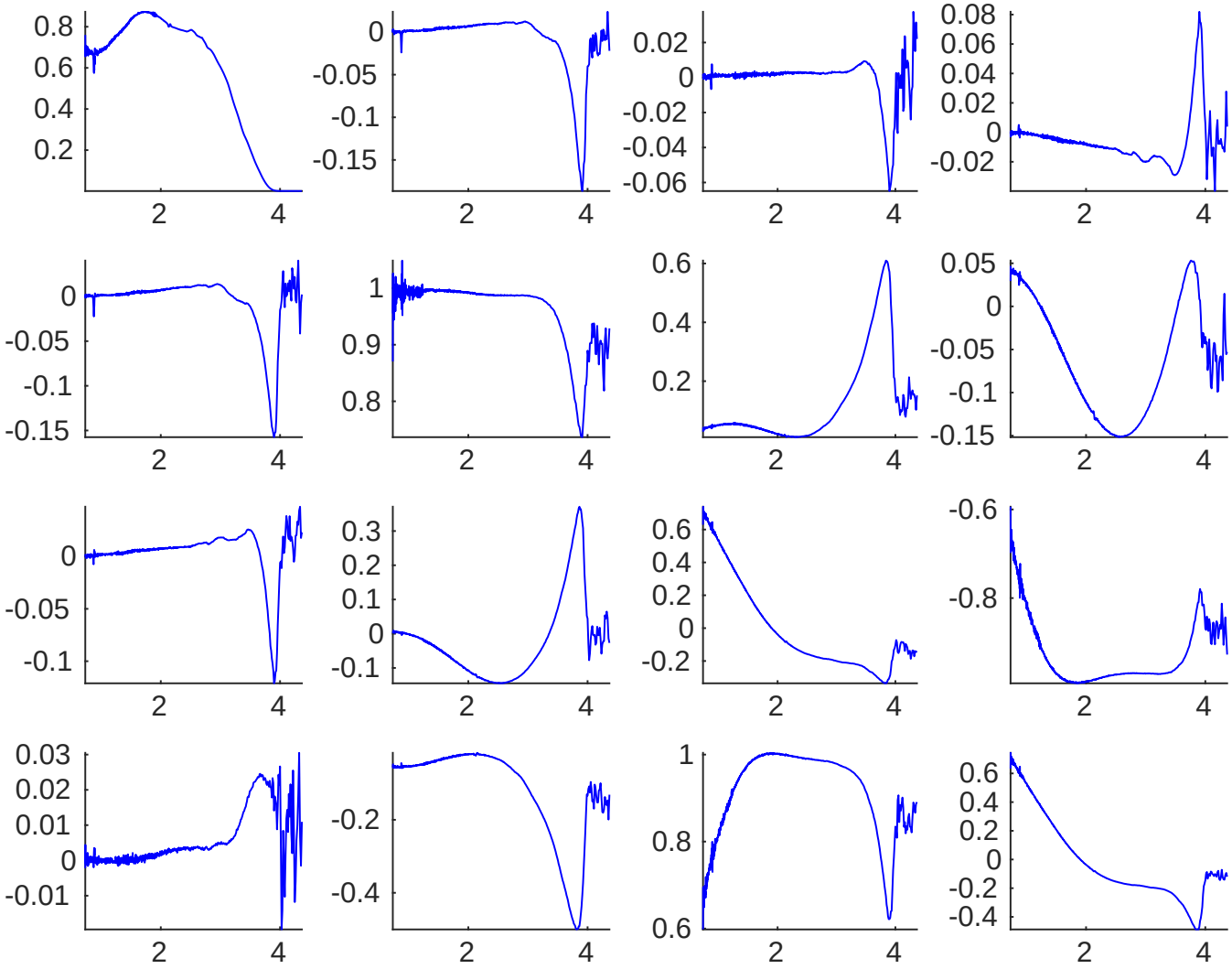

Figure 1: Müller matrix elements as a function of photon energy (eV) for an achromatic quarter-wave plate at room temperature, oriented with the fast axis aligned with the incoming polarization state.

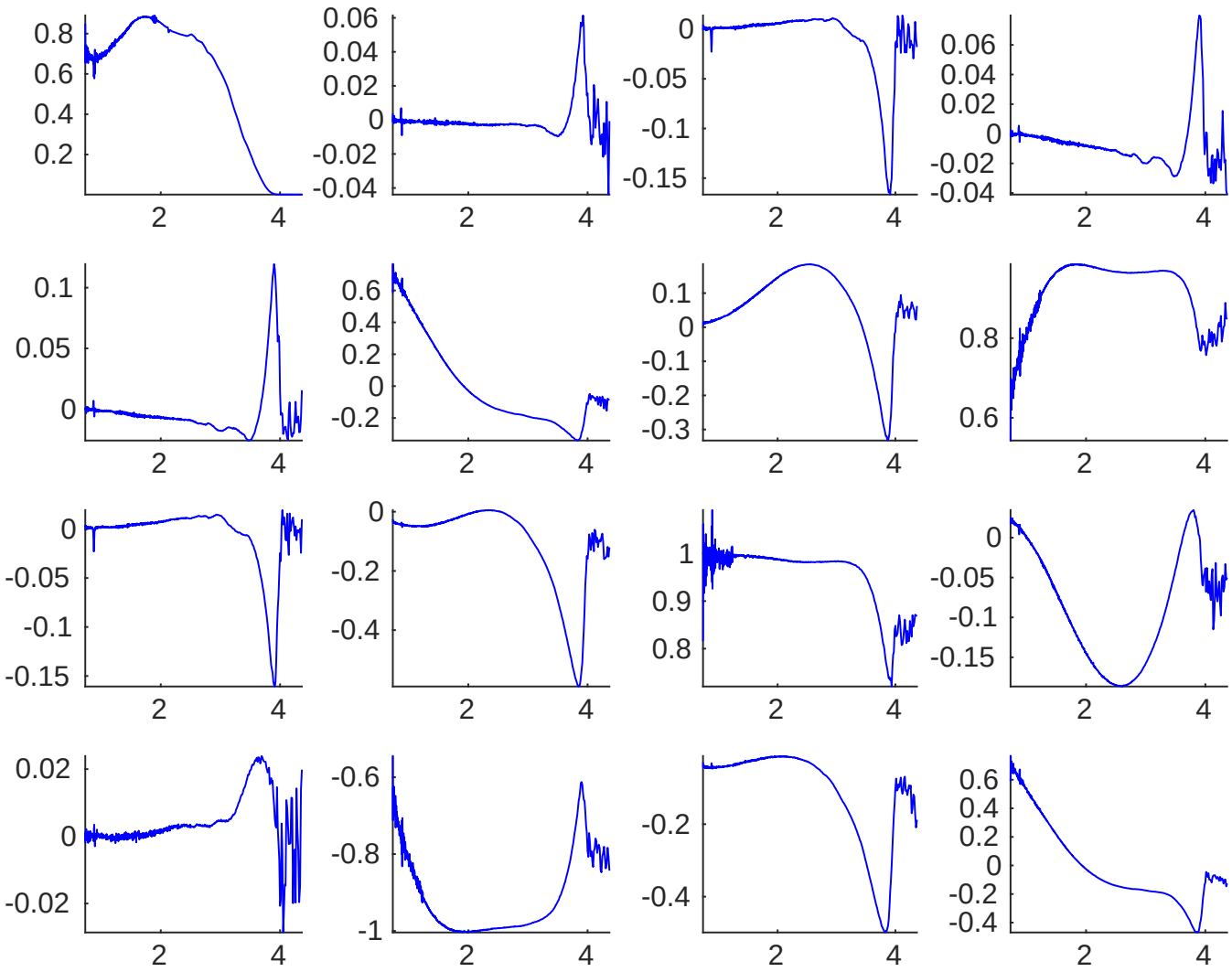

Figure 2: Müller matrix elements as a function of the photon energy (eV) for an achromatic quarter-wave plate at room temperature, oriented with 45° between incoming polarization state and fast axis.

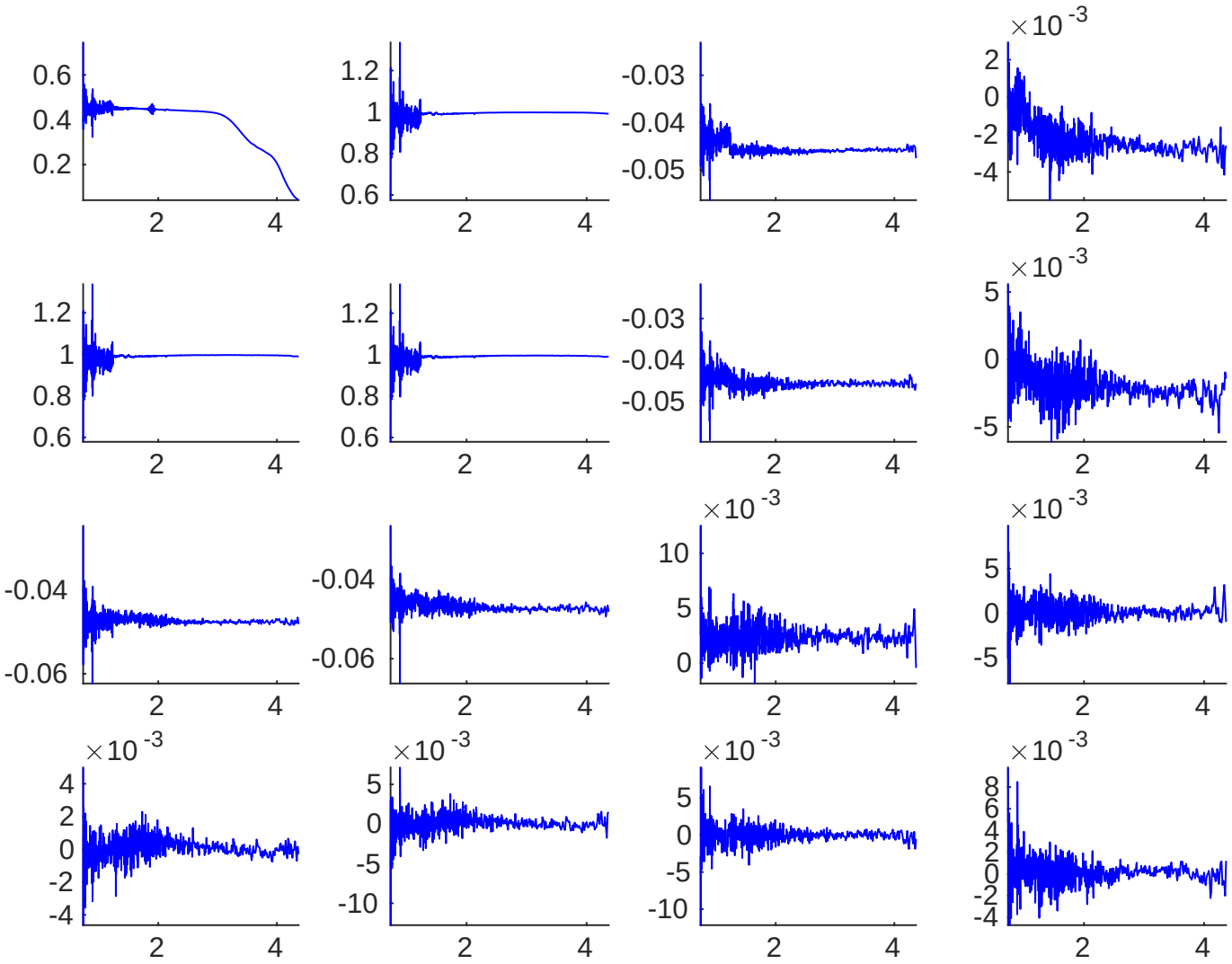

Figure 3: Müller matrix elements as a function of the photon energy (eV) for a Glan-Thompson linear polarizer with some unknown orientation with respect to the incoming polarization state.

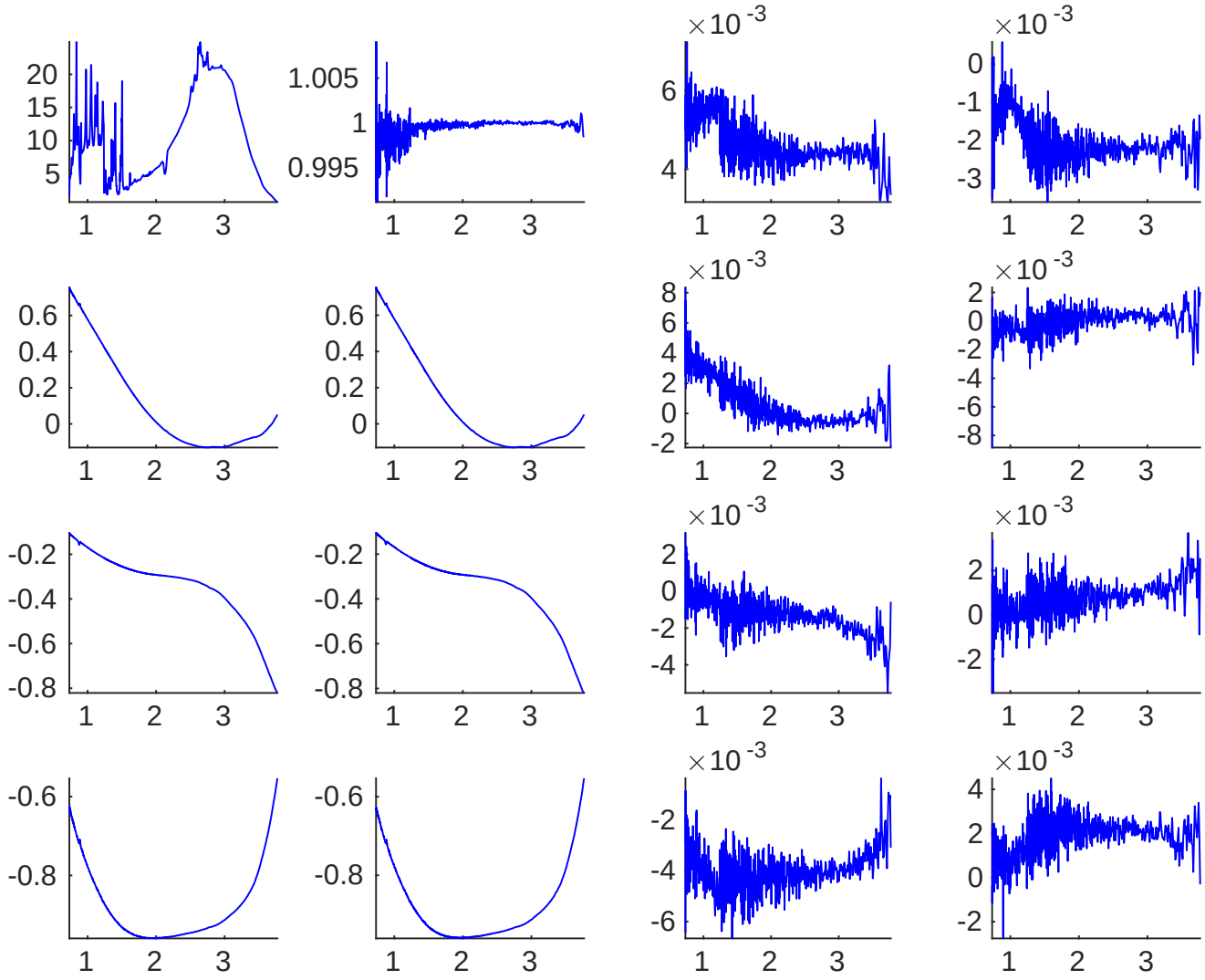

Figure 4: [a]Müller matrix elements as a function of photon energy (ev) for a composite system consisting of a Glan-Thompson linear polarizer, followed by an achromatic quarter-wave plate.

[a] This data was acquired by another lab team.

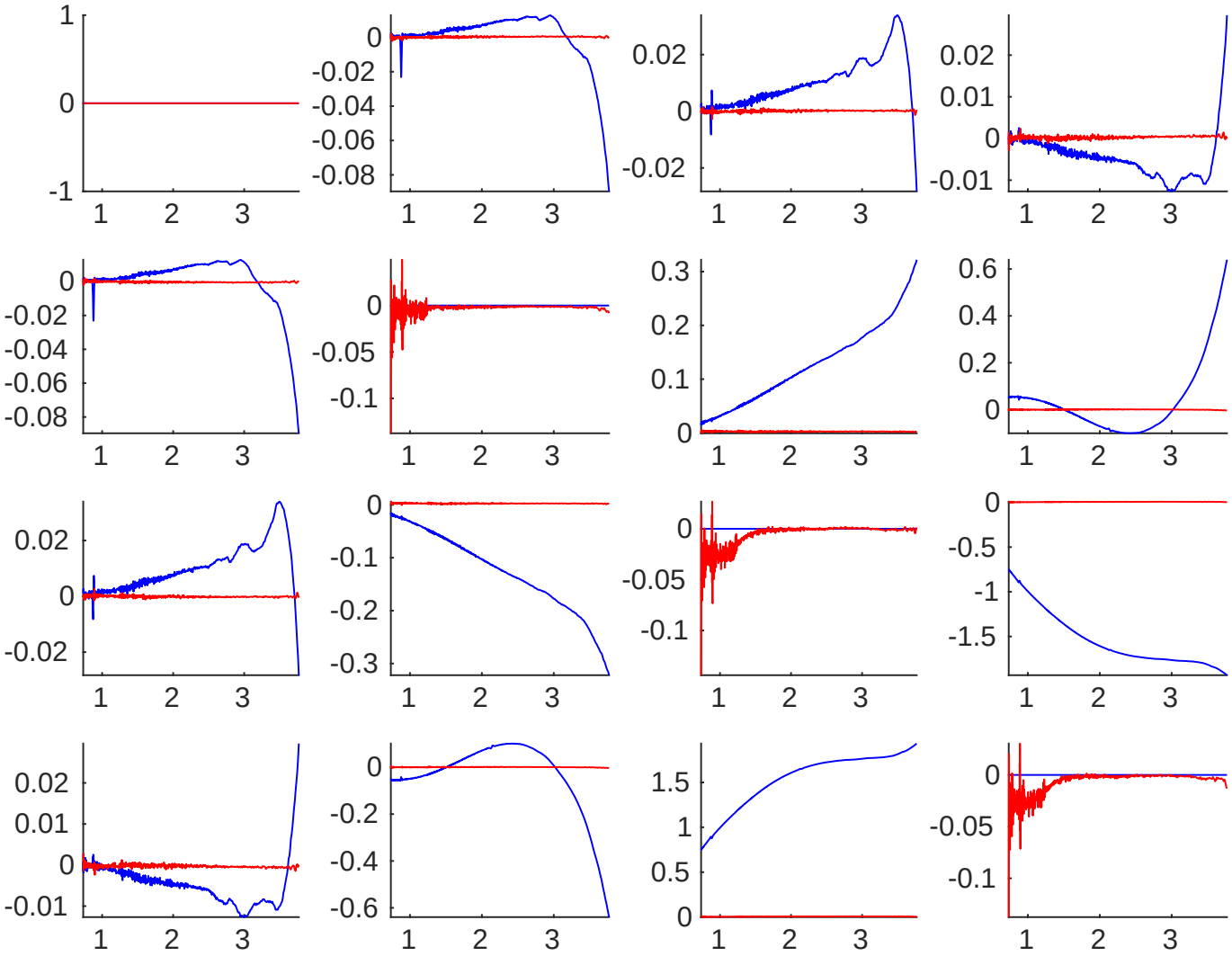

Figure 5: Differential decomposition of an achromatic quarter-wave plate with fast axis and incoming polarization state aligned. Blue: L_M. Red: L_U.

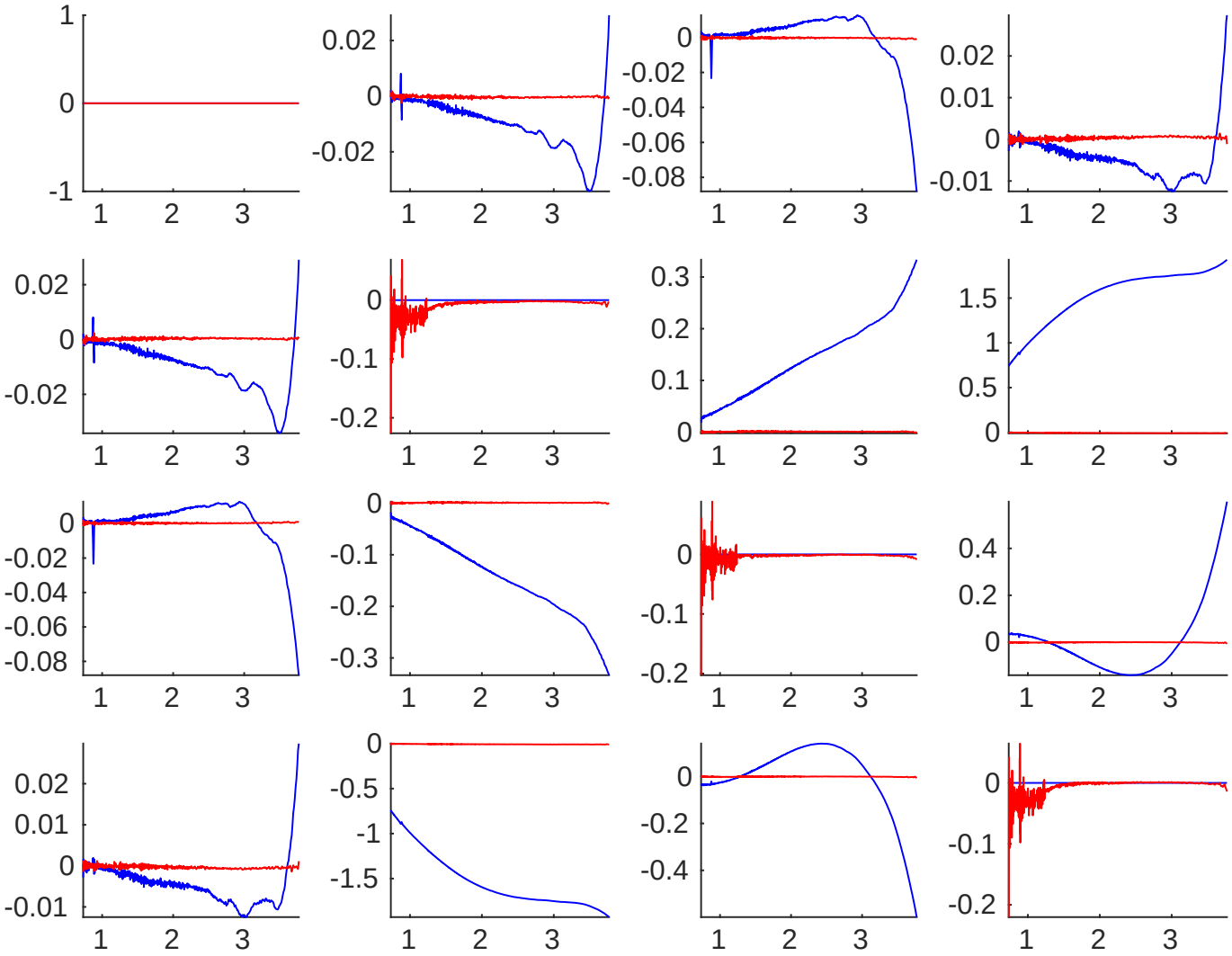

Figure 6: Differential decomposition of an achromatic quarter-wave plate with the fast axis rotated by 45° compared to the incoming polarization state. Blue: L_M. Red: L_U.

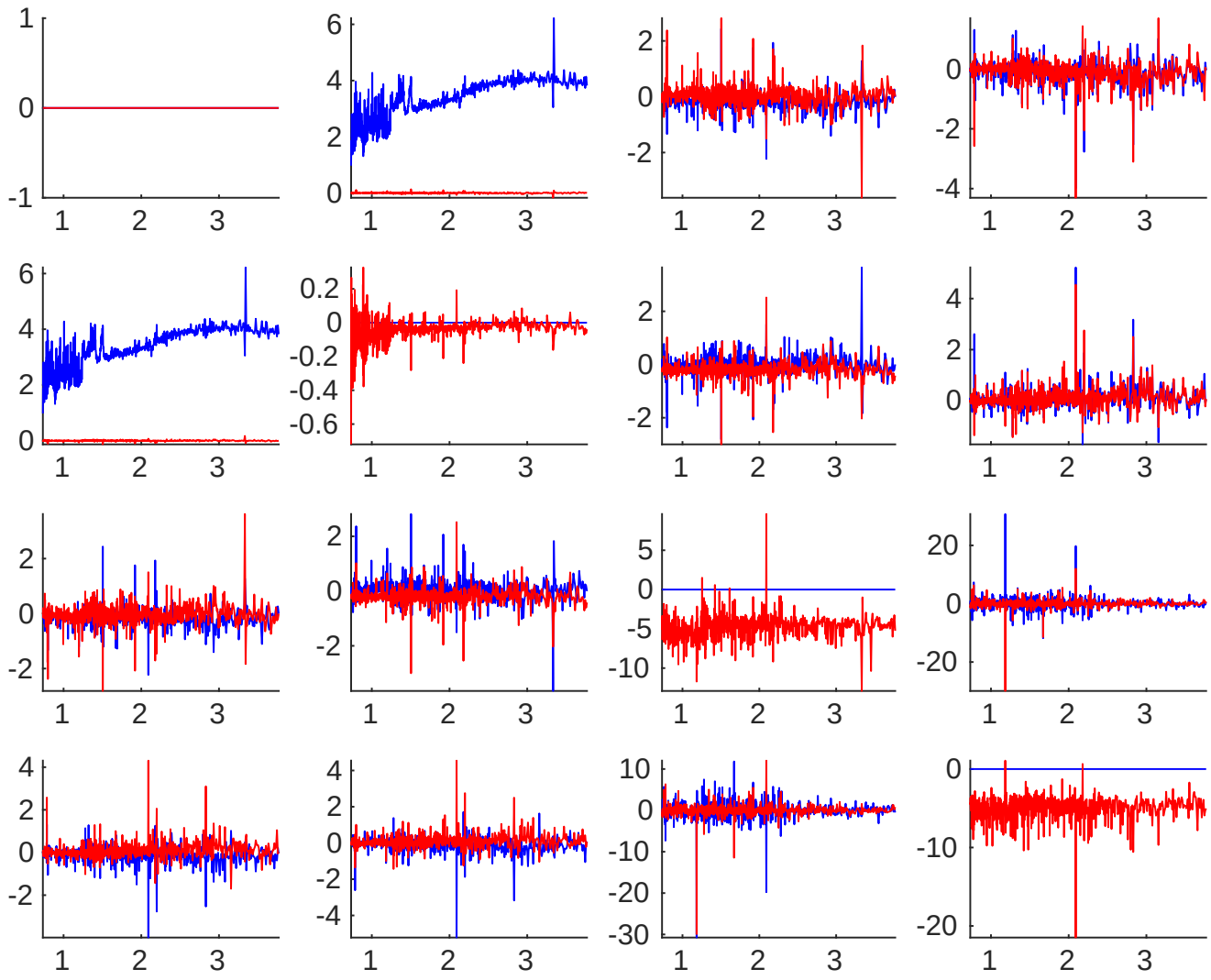

Figure 7: Differential decomposition of the Glan-Thompson linear polarizer. Blue: L_M. Red: L_U.

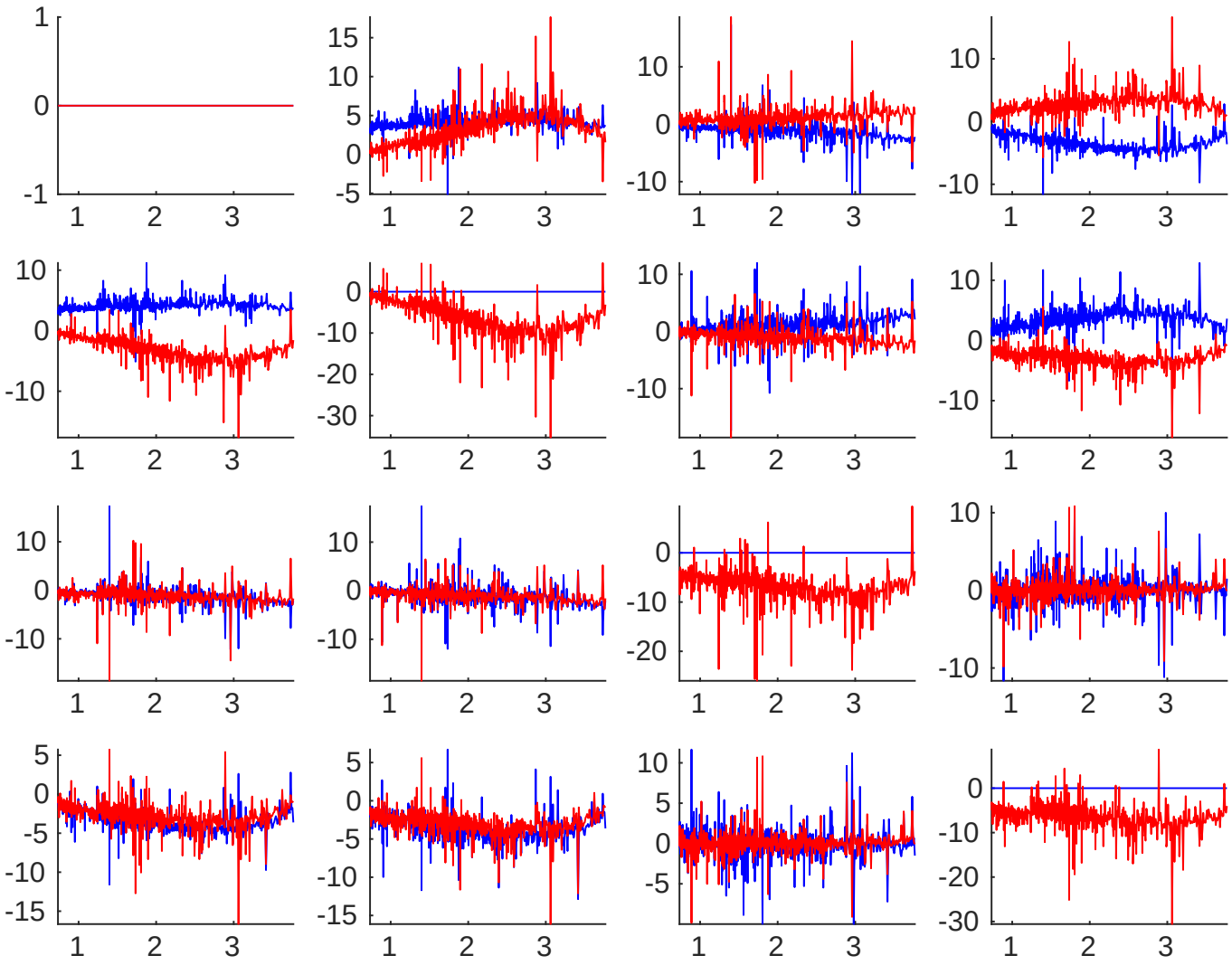

Figure 8: Differential decomposition of a composite system of a Glan-Thompson linear polarizer, and an achromatic quarter-wave plate. Blue: L_M. Red: L_U.